Combined winter climate regimes over the North Atlantic/European sector 1766–2000

C. Casty[1]
Institute of Geography, University of Bern, Bern, Switzerland

D. Handorf and M. Sempf
Alfred Wegener Institute for Polar and Marine Research, Potsdam, Germany

Received 13 January 2005; revised 18 April 2005; accepted 31 May 2005; published 1 July 2005.

[1] This paper presents combined winter climate regimes for the 1766–2000 period over the North Atlantic/European sector. We expand previous studies on recurrent regimes by combining spatially high-resolved independent reconstructions of the 500 hPa geopotential height, land surface air temperature, and precipitation fields. Nonlinear Principal Component Analysis is applied to the data in order to account for the underlying nonlinear dynamics of climate regimes. Three recurrent winter climate regimes are detected. One regime resembles in its pressure, temperature, and precipitation pattern the positive phase of the North Atlantic Oscillation, whereas the other two regimes are European blocking situations. **Citation:** Casty, C., D. Handorf, and M. Sempf (2005), Combined winter climate regimes over the North Atlantic/European sector 1766–2000, *Geophys. Res. Lett.*, *32*, L13801, doi:10.1029/2005GL022431.

1. Introduction

[2] It has long been recognized that the midlatitude planetary-scale flow is characterized by a few preferred circulation patterns [*Rossby*, 1939], which can be defined on a monthly time scale as climate regimes. The concept of climate regimes provides a framework for explaining, at least partly, low-frequency variability by transitions between distinct regimes [*Palmer*, 1999]. The concept has been proven in studies with low-order nonlinear dynamical systems, which additionally provide insight into the underlying dynamical processes [e.g., *Charney and DeVore*, 1979]. Also results from observed atmospheric data give evidence for the existence of multiple regimes for the Northern Hemisphere [*Stephenson et al.*, 2004, and references therein]. According to *Hsu and Zwiers* [2001] and *Stephenson et al.* [2004] two main requirements for identifying recurrent regimes are essential: long observational time series (exceeding the NCEP-reanalysis) and an analysis on a regional rather than on a hemispheric basis. Europe provides a large number of high-quality and long instrumental series that make this area ideal for the computation of high-resolution climate field reconstructions (CFR) [*Jones and Mann*, 2004; *Luterbacher et al.*, 2004]. In this study we perform and combine independent CFR of the 500 hPa geopotential height (Z500), land surface air temperatures (LSAT), and land surface precipitation (LSP) for the North Atlantic/European sector from 1766 to 2000. Independent means no common data are used for the reconstruction of each parameter [*Wanner and Luterbacher*, 2002; *Casty et al.*, 2005]. These reconstructions allow to study the dynamics and interactions between climate variables on a much longer time scale than offered by the reanalyses period. The detection of climate regimes is usually performed on monthly 500 hPa geopotential height data [*Corti et al.*, 1999; *Palmer*, 1999; *Stephenson et al.*, 2004]. In this study we extend previous analyses by investigating combined fields (comprising Z500, LSAT, and LSP) with the aim of a more comprehensive dynamical characterization of the climate regimes over time. We focus on winter (D, J, F) data as the main patterns of variability are more pronounced for the North Atlantic/European sector during that season. In order to detect combined winter climate regimes and to account for its nonlinear dynamics, Nonlinear Principal Component Analysis (NLPCA) [*Monahan*, 2000] is applied in the 10-dimensional state space spanned by the combined linear Principal Component Analysis patterns (CLPCA) [e.g., *Bretherton et al.*, 1992].

2. Data and Methods

[3] We independently reconstructed monthly North Atlantic/European Z500, LSAT, and LSP gridded climate fields back to 1766 through Principal Component (PC) regression. CFR seeks to reconstruct a large-scale field by regressing a spatial network of station data against instrumental field information [*Jones and Mann*, 2004, and references therein]. During periods when both, station and field information (reanalysis) are available, regression models are developed within the 20th century and fed with station data prior to the reanalysis period to reconstruct past climate fields under the assumption of stationarity ('paleoreanalysis'). The spatial resolution is given by 2.5° × 2.5° (0.5° × 0.5°) covering the area 30–80°N and 50°W–40°E for Z500 (LSAT and LSP). The choice of this area was motivated by fully capturing the extension of the main pattern of atmospheric variability in this sector, the North Atlantic Oscillation (NAO). For Z500 reconstructions, NCEP reanalysis [*Kalnay et al.*, 1996; *Kistler et al.*, 2001] is used for calibration/verification and CRU TS 2.0 for LSAT and LSP [*Mitchell et al.*, 2004]. The PC-regression approaches for Z500 reconstructions are described by *Luterbacher et al.* [2002], for LSAT by *Luterbacher et al.* [2004], and for LSP by A. Pauling et al.

[1]Now at Physics Institute, University of Bern, Bern, Switzerland.

0094-8276/05/2005GL022431$05.00

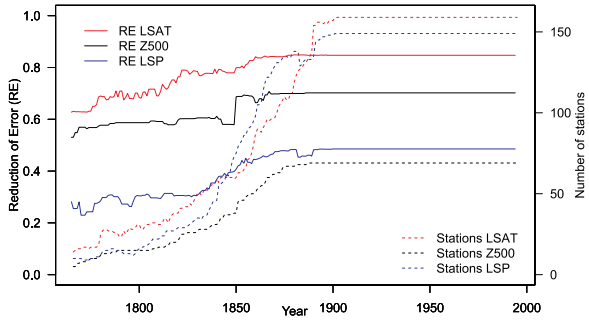

Figure 1. Spatially averaged Reduction of Error (RE) values for the winters (DJF) 1766–1995 (solid lines, left *y*-axis). The range of RE is $-\infty$ to 1. 1 indicates a perfect reconstruction, 0 means the reconstruction is not better than climatology. −1 is a random guess. The calibration period for the Z500 reconstruction (LSAT and LSP) is given by 1948–1975 (1901–1960). The verification period for the calculation of the RE ranges from 1976–1995 (1961–1995) for Z500 (LSAT and LSP). The evolution of the number of station data for each reconstruction is plotted with dotted lines (right *y*-axis). The total number of stations is 69 for Z500, 159 for LSAT, and 149 for LSP.

(500 years of gridded high-resolution precipitation reconstructions over Europe and the connection to large-scale circulation, submitted to *Climate Dynamics*, 2005. For our independent approach (reconstructions share no common station data) the CFR relies entirely on measured station time series (e.g., temperature stations for LSAT CFR Sea level pressure stations for 2500, and precipitation for LSP). The minimum number of station data was set to five to assure overall reliable performance of the reconstructions (Figure 1). 176 nested regression models are developed to reconstruct Z500, 422 models for the LSAT, and finally 373 for the LSP in order to account for the changing number of station series over time. Note that for Z500 (LSAT and LSP) the data from 1948 (1901) onwards are the reanalyses themselves. Spatially averaged verification results (Reduction of Error, RE) [*Lorenz*, 1956] for winter (DJF) and the evolution of the number of station data are plotted in Figure 1 (see also supporting material[1]).

[4] For compatibility reasons, LSAT and LSP reconstructions are interpolated on the 2.5° grid of Z500. For each variable, normalized anomalies are calculated by subtracting the 1766–2000 mean annual cycle and dividing by the standard deviation. Then, the CFR of 777 grid points each (LSAT and LSP incorporate 444 grid points over land) are comprised into a combined climate state vector of normalized winter (D, J, F) data [*Fraedrich et al.*, 1993] of 705 time steps. In order to detect climate regimes, NLPCA [*Monahan*, 2000] is applied in the space spanned by the first 10 leading CLPCA modes accounting for 76.7% of the total combined variance. The first NLPCA mode is characterized by a curve in this 10-dimensional space and corresponds to a sequence of spatial maps. The temporal evolution along the NLPCA1 curve can be characterized by a time series $\lambda(t)$, which measures the distance along the curve to one endpoint of

[1]Auxiliary material is available at ftp://ftp.agu.org/apend/gl/2005GL022431.

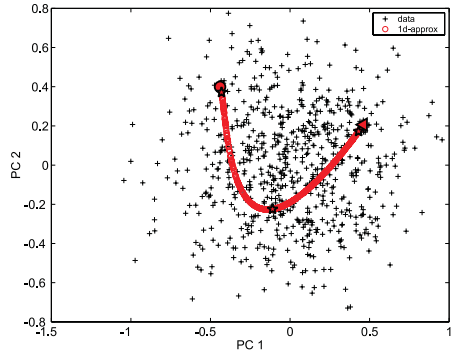

Figure 2. NLPCA1 mode for monthly winter (D, J, F) reconstructed data projected onto the leading two CLPCA modes. The symbols ⋆ indicate the positions of the climate regimes in the state space. The symbol (△) indicates the starting (end) point of the NLPCA1 curve.

the NLPCA1 curve. This time series is an analog to the linear PC time series. Recurrent climate regimes are then defined as patterns in the state space, which correspond to maxima of the probability density function (PDF) of $\lambda(t)$. Here, the PDF has been calculated with a Gaussian kernel estimator with conservative settings for all parameters to avoid spurious multimodality [*Silverman*, 1986].

3. Results

[5] The Z500 and LSAT reconstructions perform very well (high overall RE values) and moderately for LSP. The quality increases with the number of station information (Figure 1). Europe with its high-density station network is better reconstructed than regions at the margins of the studied area (not shown). Figure 2 shows the first NLPCA mode plotted in the space spanned by the first two CLPCA modes. The NLPCA1 is an u-shaped curve, which is mainly situated in the PC1/PC2 plane in our case. The NLPCA1 mode explains 28.1% of total variance compared to 25.2% for CLPCA1. The statistical robustness of the first NLPCA mode has been proven by studying the sensitivity of the NLPCA approximation to input data contaminated with noise. Therefore, 10D series of Gaussian random deviates with the same mean and standard deviation as the input data have been multiplied by a noise

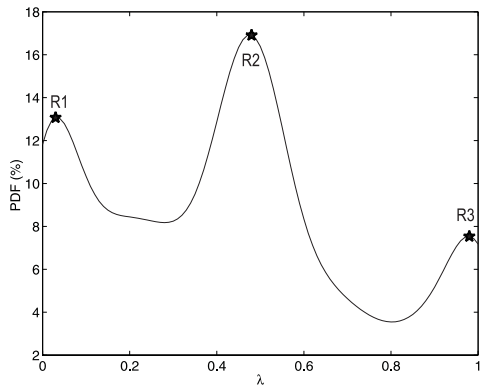

Figure 3. PDF (in %) of the NLPCA1 time series $\lambda(t)$. The symbols ⋆ indicate the maxima of the PDF. The regimes are labeled R1–R3.

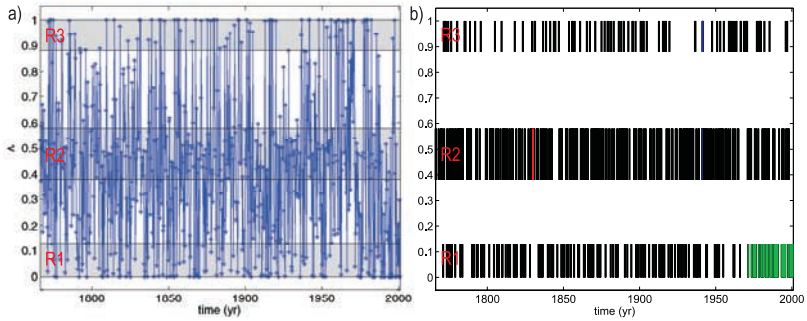

Figure 4. (a) The time series of the NLPCA1 $\lambda(t)$. The gray shadings mark the $\lambda(t)$-intervals of the recurrent climate winter regimes detected in Figures 2 and 3. (b) The same as Figure 4a but a bar code for the members $\lambda(t)$ that are classified as a climate regime is plotted. It represents the occurrence of $\lambda(t)$ in either one of the regimes. The transitions are masked out. The winters of 1830 (red), 1941 (blue), and R1 regimes since 1970 (green) are colored.

level η and added to the input data. The NLPCA is repeated and the u-shaped NLPCA1 remains robust until a noise level of 10%. Figure 3 presents the Gaussian kernel estimation of the PDF of the time series $\lambda(t)$. This time series measures the distance to the starting point of the NLPCA1 curve, which is indicated by the symbol $\triangle$ in Figure 2. The PDF reveals three maxima, indicated by the symbols $\star$ and lettered R1–R3, which are located at $\lambda = 0.03$, $\lambda = 0.48$ and $\lambda = 0.98$. As described by *Monahan et al.* [2001], the corresponding atmospheric states are identified as recurrent climate regimes. The time series of $\lambda(t)$ itself is displayed in Figure 4a. λ-intervals of [0, 0.13] for R1, [0.38, 0.58] for R2, and [0.88, 1] for R3 (gray-shadings in Figure 4a) can be considered as indicators for climate regimes. These intervals have been subjectively chosen by a threshold of ±0.1 around the PDF-maxima of λ, taking into account that $\lambda \in [0, 1]$. The results of the regime analysis have been proven to being robust for reasonable changes in the boundaries of the intervals, as it was emphasized in *Monahan et al.* [2003]. To better visualize the occurrence of the regimes, Figure 4b is introduced.

[6] The spatial maps of the climate regimes (Figure 5) can be derived from the 10-dimensional CLPCA coordinate vectors of those points of the NLPCA1 curve, which correspond to the maxima of the PDF. The position of the climate regimes on the NLPCA1 curve is indicated by the symbols $\star$ in Figure 2.

[7] The Z500 anomaly pattern of R1 exhibits a zonal flow regime (Figure 5a). Positive geopotential height anomalies over south-western Europe coincide with negative ones over Iceland, leading to an enhanced anomalous westerly flow of mild and wet air towards central Europe. This is supported by the independent LSAT and LSP fields for R1 (Figures 5b and 5c). The LSAT exhibits positive temperature anomalies over northern, central, and eastern Europe and below normal values over Greenland. The LSP pattern of R1 (Figure 5c) is characterized by strong positive precipitation anomalies for central and northern Europe, which are centered over the British Isles. Negative precipitation is found south of around 40°N. Thus, the R1 regime resembles the well-known positive phase of the NAO in Z500 and its corresponding seesaw in temperatures between Greenland and Northern Europe [*van Loon and Rogers*, 1978]. The temporal behavior (Figures 4a and 4b) indicates the existence of periods with pronounced occurrence of the R1 regime (e.g. 1805–1825, since 1970) as well as time segments when R1 did not appear (e.g., 1828–1833, 1886–1890, 1955–1962).

[8] The regime R2 shows positive geopotential height anomalies centered over Scandinavia and negative ones south of around 45° (Figure 5d). The magnitude of the Z500 anomalies is much smaller compared to R1 and R3. R2 is connected with anomalous cold air advection from western Russia towards central Europe (Figure 5e). The anomalous easterly flow is also related to below normal winter precipitation over most areas of Europe, except the Mediterranean (Figure 5f). Due to the position of this regime close to the mean climate state, it is the most frequent (Figures 3, 4a, and 4b). Nevertheless, time segments of several years length can be detected, when the regime R2 was not present (e.g., 1784–1790, 1843–1848, 1965–1970).

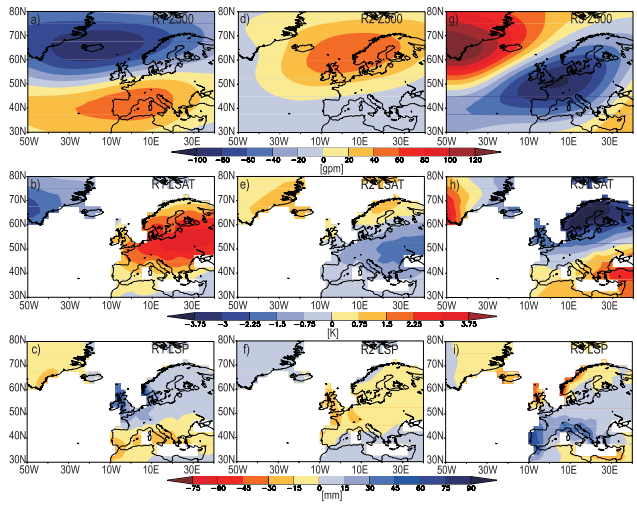

Figure 5. (a–i) Anomaly patterns (reference period 1766–2000) of the combined winter climate regimes for the North Atlantic/European area 1766–2000 indicated in Figure 2 by the symbols $\star$. Anomalies are given in geopotential meters [gpm], Kelvin [K], and millimeters [mm], respectively.

[9] The combined climate winter regime R3 has a dipole structure in the Z500 anomaly pattern (Figure 5g). Anomalously low Z500 values stretch form the eastern North Atlantic over Europe towards western Russia. Positive Z500 anomalies are found over the northwestern sector of the studied area. This leads to a northeasterly flow anomaly offshore of Europe and a southwesterly flow towards southeastern Europe. Northern Europe is affected by cold and dry polar air masses (Figures 5h and 5i) whereas Spain and Italy are influenced by warmer and wetter conditions than average. R3 is the least frequent of the three detected regimes (Figure 3). Again, periods dominated by R3 (e.g., 1958–1971) as well as longer time segments up to more than 10 years without any occurrence of R3 (e.g., 1796–1805, 1919–1936) are found (Figures 4a and 4b).

4. Discussion and Summary

[10] We detected three recurrent winter climate regimes in combined fields of Z500, LSAT, and LSP in the North Atlantic/European sector 1766–2000 using NLPCA. This method allows not only the detection of the corresponding regime flow patterns but elucidates inherently their temporal structure regarding occurrence and regime transitions.

[11] The R1 regime resembles the positive phase of the NAO, whereas R2 and the R3 regime reveal blocking conditions for Europe.

[12] During the interpretation process, one has to be aware of the changing quality of the reconstruction over time. Due to the dense station network in Europe the Z500 and LSAT CFR presented in this study perform very well. For LSP, during the period 1766–1800 the spatially averaged RE is around 0.3, but with a nonuniform spatial distribution. For western, central and northwestern Europe the distribution of the RE reveals skillful reconstructions with values up to 0.9 (not shown). However, some parts of the Mediterranean and southern Greenland have skill lower than climatology. The interpretation for the precipitation patterns should therefore be made with caution during periods with lowered REs, especially prior to 1800.

[13] The detected temporal regime evolution provide the possibility for further detailed studies on the attribution of specific winter regime conditions to pronounced climate anomalies known from proxy and observational data even for times long before the start of the observational period. Three examples are briefly discussed here. 1830, the coldest Alpine winter over the last 500 years [*Casty et al.*, 2005] was characterized by a persistent R2 regime over Europe for the three winter months, which also lead to dry conditions (red markers in Figure 4b). The winter 1941 as the high phase of the cold anomaly winters 1940–1942 [*Brönnimann et al.*, 2004] was characterized by a transition from R2 in December 1940 to a persistent R3 for January and February 1941 (blue in Figure 4b). The pronounced occurrence of the R1 regime since the 1970s (34 times; green in Figure 4b) led to warm and wet winters in central Europe [*Hurrell and van Loon*, 1997]. It is very likely that the last 30 winters were the warmest in Europe over the last 500 years [*Luterbacher et al.*, 2004].

[14] The independent CFR allow studying the dynamics of such extremes in the past. The classification of atmospheric variability into climate regimes and transitions between them has a potential to significantly improve monthly to seasonal climate forecast. This would be possible, for example, by applying a Markov chain model that accounts for the probabilities of occurrence in either one of the regimes or its transitions [*Vautard et al.*, 1990]. Furthermore, the detection of climate regimes over the North Atlantic/European sector is no longer restricted to the NCEP period since 1948.

[15] **Acknowledgment.** We thank the Swiss National Science Foundation through its National Center in Competence (NCCR) in Climate and the Marchese Francesco Medici del Vascello Foundation for financial support. Carlo Casty is funded by the European Commission under the fifth framework Programme, Contract EVRI-2002-000413, Project PACLIVA.

References

Bretherton, C. S., C. Smith, and J. M. Wallace (1992), An intercomparison of methods for finding coupled patterns in climate data, *J. Clim.*, *5*, 541–560.

Brönnimann, S., J. Luterbacher, J. Staehelin, T. M. Svendby, G. Hansen, and T. Svenøe (2004), Extreme climate of the global troposphere and stratosphere in 1940–1942 related to El Niño, *Nature*, *431*, 971–974.

Casty, C., H. Wanner, J. Luterbacher, J. Esper, and R. Böhm (2005), Temperature and precipitation variability in the European Alps since 1500, *Int. J. Climatol.*, in press.

Charney, J. G., and J. G. DeVore (1979), Multiple flow equilibria in the atmosphere and blocking, *J. Atmos. Sci.*, *36*, 1205–1216.

Corti, S., F. Molteni, and T. N. Palmer (1999), Signature of recent climate change in frequencies of natural atmospheric circulation regimes, *Nature*, *398*, 799–802.

Fraedrich, K., C. Bantzer, and U. Burkhardt (1993), Winter climate anomalies in Europe and their associated circulation at 500 hPa, *Clim. Dyn.*, *8*, 161–175.

Hsu, C. J., and F. Zwiers (2001), Climate change in recurrent regimes and modes of Northern Hemisphere atmospheric variability, *J. Geophys. Res.*, *106*, 20,145–20,159.

Hurrell, J. W., and H. van Loon (1997), Decadal variations associated with the North Atlantic Oscillation, *Clim. Change*, *36*, 301–326.

Jones, P. D., and M. E. Mann (2004), Climate over past millennia, *Rev. Geophys.*, *42*, RG2002, doi:10.1029/2003RG000143.

Kalnay, E., et al. (1996), The NCEP/NCAR 40-year reanalysis project, *Bull. Am. Meteorol. Soc.*, *77*, 437–471.

Kistler, R., et al. (2001), The NCEP-NCAR 50-year reanalysis: Monthly means CD-ROM and documentation, *Bull. Am. Meteorol. Soc.*, *82*, 247–267.

Lorenz, E. N. (1956), Empirical orthogonal functions and statistical weather prediction, *Stat. Forecast Proj. Rep. 1*, Dep. of Meteorol., Mass. Inst. of Technol., Cambridge.

Luterbacher, J., et al. (2002), Reconstruction of sea level pressure fields over the Eastern North Atlantic and Europe back to 1500, *Clim. Dyn.*, *18*, 545–561.

Luterbacher, J., D. Dietrich, E. Xoplaki, M. Grosjean, and H. Wanner (2004), European seasonal and annual temperature variability, trends and extremes since 1500, *Science*, *303*, 1499–1503.

Mitchell, T. D., T. R. Carter, P. D. Jones, M. Hulme, and N. New (2004), A comprehensive set of high-resolution grids of monthly climate for Europe and the globe: The observed record (1901–2000) and 16 scenarios (2001–2100), *Working Pap. 55*, Tyndall Cent. for Clim. Change, Norwich, U. K.

Monahan, A. H. (2000), Nonlinear principal component analysis by neural networks: Theory and application to the Lorenz system, *J. Clim.*, *13*, 821–835.

Monahan, A. H., L. Pandolfo, and J. C. Fyfe (2001), The preferred structure of variability of the Northern Hemisphere atmospheric circulation, *Geophys. Res. Lett.*, *28*, 1019–1022.

Monahan, A. H., J. C. Fyfe, and L. Pandolfo (2003), The vertical structure of wintertime climate regimes of the Northern Hemisphere extratropical atmosphere, *J. Clim.*, *16*, 2005–2021.

Palmer, T. N. (1999), A nonlinear perspective on climate change, *J. Clim.*, *12*, 575–591.

Rossby, C. G. (1939), Relation between variations in the intensity of the zonal circulation of the atmosphere and the displacement of the semi-permanent centers of action, *J. Mar. Res.*, *2*, 38–55.

Silverman, B. W. (1986), *Density Estimation for Statistics and Data Analysis*, CRC Press, Boca Raton, Fla.

Stephenson, D. B., A. Hannachi, and A. O'Neill (2004), On the existence of multiple climate regimes, *Q. J. R. Meteorol. Soc.*, *130*, 583–606.

van Loon, H., and J. C. Rogers (1978), The seesaw in winter temperatures between Greenland and Northern Europe. Part I: General description, *Mon. Weather Rev.*, *106*, 296–310.

Vautard, R., K. C. Mo, and M. Ghil (1990), Statistical significance test for transition matrices of atmospheric Markov chains, *J. Atmos. Sci.*, *47*, 1926–1931.

Wanner, H., and J. Luterbacher (2002), The LOTRED approach – A first step towards a "paleoreanalysis" for Europe, *PAGES News*, *10*, 9–11.

C. Casty, Physics Institute, University of Bern, Sidlerstrasse 5, CH-3012 Bern, Switzerland. (casty@climate.unibe.ch)

D. Handorf and M. Sempf, Alfred Wegener Institute for Polar and Marine Research, Telegrafenberg A 43, D-14473 Potsdam, Germany.

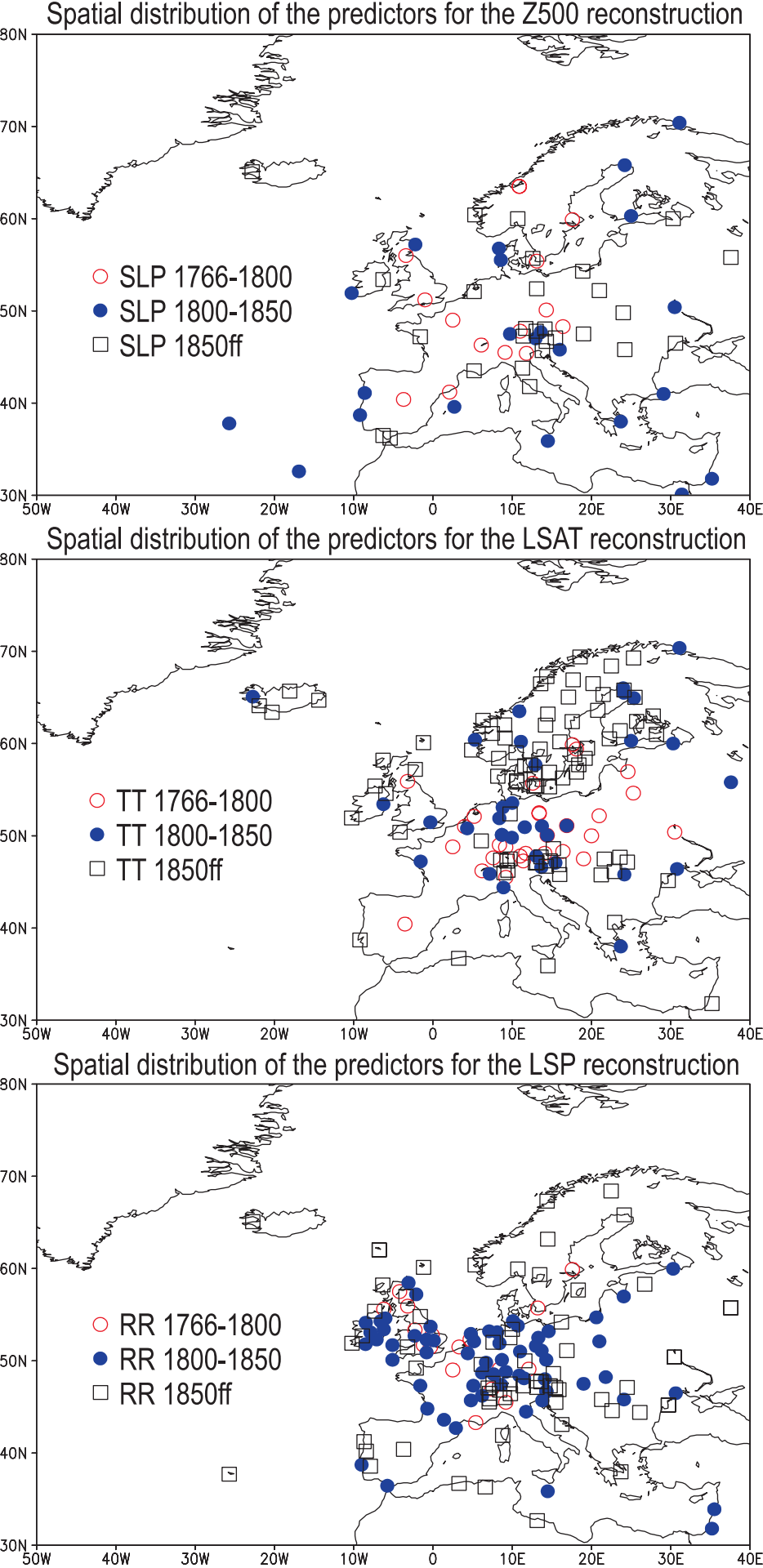

Figure A: The spatial distribution of the station data used for the independent monthly reconstruction of Z500 (top), LSAT (middle), and LSP (bottom) for the period 1766-2000 over the North Atlantic/European sector. Sea level pressure (SLP) station data are used for the Z500 reconstruction, land surface temperatures (TT) for the LSAT, and finally land precipitation measurements (RR) for LSP. The distribution of the station data is plotted for three time windows (1766-1800, 1800-1850, 1850 onwards) in order to visualize the temporal evolution of the station network.